A high-voltage triggered pseudospark discharge experiment

K. Ramaswamy, W. W. Destler, and J. Rodgers
Electrical Engineering Department and Institute of Plasma Research, University Of Maryland, College Park, Maryland 20742

(Received 22 January 1996; accepted for publication 22 July 1996)

The design and execution of a pulsed high-voltage (350–400 keV) triggered pseudospark discharge experiment is reported. Experimental studies were carried out to obtain an optimal design for stable and reliable pseudospark operation in a high-voltage regime (>350 kV). Experiments were performed to determine the most suitable fill gas for electron-beam formation. The pseudospark discharge is initiated by a trigger mechanism involving a flashover between the trigger electrode and hollow cathode housing. Experimental results characterizing the electron-beam energy using the range-energy method are reported. Source size imaging was carried out using an x-ray pinhole camera and a novel technique using Mylar as a witness plate. It was experimentally determined that strong pinching occurred later in time and was associated with the lower-energy electrons. © *1996 American Institute of Physics.* [S0021-8979(96)00321-0]

I. INTRODUCTION

The pseudospark is a low-pressure gas discharge in a hollow cathode and a planar anode configuration operating on the left-hand branch of a characteristic breakdown curve which is similar to the Paschen curve for parallel electrodes. This phenomenon was first reported by Christiansen and Schultheiss.[1]

The pseudospark discharge has several interesting features and one important feature has been the observance of highly pinched electron beams with current densities of up to 10^6 A/cm^2 during the breakdown phase. Interest in these electron beams has been stimulated by their potential applications in such diverse areas as thin-film fabrication[2] and materials processing.[3]

Several experiments have been reported[4–6] over the last decade in which high-brightness electron beams have been produced in pseudospark devices operating in the voltage range 20–50 kV. The extraction of these ion-focused, high-current-density electron beams into vacuum requires the generation of these beams at energies comparable to those achieved in the field-emission diodes associated with pulse line accelerators.[7,8] With this objective in mind, we reported experiments[7,9] wherein a high-power pulse line accelerator was mated to a hollow cathode discharge experiment operating in the pseudospark regime. In those experiments, reliable operation beyond 200 kV proved difficult due to frequent field-emission-induced high-voltage breakdown. In this article we report a high-voltage triggered pseudospark wherein we have been able to scale the the voltage to 400 kV. The device operates reliably at these voltages. As the device is triggered, the device operation is well controlled.

The article is organized as follows. The experimental setup is described in Sec. II and experiments are described in Sec. III. In Sec. IV, the experimental results are discussed and finally the conclusions are drawn in Sec. V.

II. EXPERIMENTAL SETUP

In this section the power supply, the trigger circuit, the design of the multigap pseudospark assembly, and the diagnostics are described.

A. Power supply

A quasi-dc (long pulse 35 μs), high-voltage (500 kV), unipolar power supply was built using a 1:16 high-voltage pulse transformer. The equivalent circuit of the power supply (with respect to the primary side of the pulse transformer) is shown in Fig. 1. The transformer is represented as a combination of a shunt primary inductance of value equal to 400 μH and a series leakage inductance of value equal to 2 μH. The power supply is essentially an LC circuit with a switch (a triggered spark gap). The storage capacitor C (0.68 μs) is charged with the help of an external dc power supply. An external inductor (L_{ext}=264 μH) and the primary of the transformer constitutes the total inductance L. The diode in the primary circuit clips any positive swing of the voltage wave form. The voltage on the primary is stepped up by the 1:16 pulse transformer to the required high voltage. The pseudospark is connected to the secondary of the transformer by a charging resistance equal to 9 kΩ (~32 Ω primary side).

B. Design of the pseudospark assembly

The main design requirements are that the pseudospark multigap assembly should have the ability to withstand high voltages (>300 kV) and reliable long-path gas breakdown should take place only along the central axis originating from the hollow cathode and terminating through the anode hole (pseudospark regime). Also, the design of the system should be sufficiently simple so that it can be fabricated easily facilitating quick modifications.

Poor reliability of our earlier design[7,9] beyond 200 kV constituted the main driving force behind our new approach. In the earlier design the electrode-to-electrode distance was 0.635 cm in the multigap arrangement. Each electrode had a 0.635-cm-diam aperture. It was thought that by increasing the number of gaps in a multigap system one could reduce the macroscopic field and thus operate at higher voltages. However, it was observed that by increasing the effective anode–cathode distance (increasing the number of gaps), the pressure regime became low with the effect that the pseu-

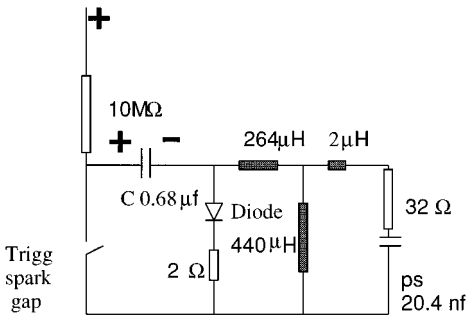

FIG. 1. Basic power supply circuit.

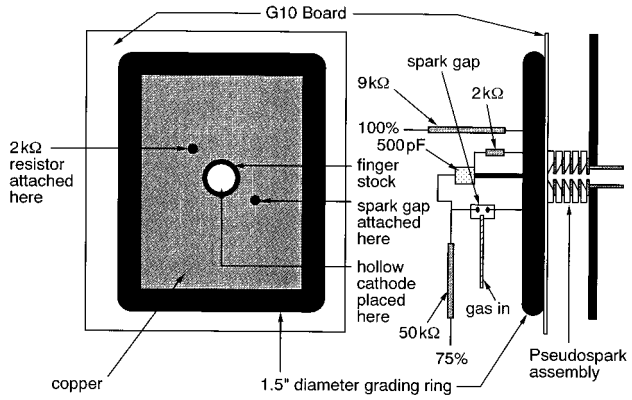

FIG. 2. Pseudospark assembly showing the external capacitor, multigap pseudospark device, and the connections to the pulse transformer.

dospark discharge in the self-breakdown mode was very erratic and also the pseudospark multigaps often broke down successively in a domino manner. This resulted in higher voltages being applied over a successively shorter distance. This invariably reduced the lifetime of the device.

A new design approach was employed here. The strategy was to keep the distance of the anode cathode around 8–10 cm (sufficient ambient gas pressure) and to decrease the number of multigaps by increasing the insulator thickness and reducing the thickness of the floating electrodes. This would have the effect of reducing the local electric fields near the triple point (metal–insulator–gas interface) and also reduce the probability of surface breakdown along the insulator.

The thickness of the floating electrode was 0.32 cm. Initially, the insulator thickness was 2.3 cm. Using this thickness no pinching of the electron beam was observed and on examining the system no evidence was found of activity around the hollow cathode. This was also the case for 1.9 cm, too, however, when the thickness was around 1.3 cm, evidence of pinched electron beam was seen (radio chromic paper, copper foil witness plate). When the insulator thickness was greater than 1.3 cm discharge took place when the device was subjected to high voltage; however, it was not clear whether the long path discharge took place along the central axis with the hollow cathode playing a role. Lack of activity near the cathode aperture and no pinching of electron beams suggested that the discharge did not originate near the cathode aperture/hollow cathode region. It should be noted that in the case of finite duration pulse charged high-voltage device, collapse of voltage cannot be a good criterion of pseudospark discharge as voltage collapse can also be initiated due to field-induced electron emission. Note that, during these investigations, the pseudospark was operated in the self-breakdown mode.

An explanation for the successful operation at this particular thickness and aspect ratio (aperture size 0.635 cm) can be found in Liu and Rhee's scaling law for a single gap system.[10] They experimentally determined that if the anode cathode distance d was more than $3D$, where D is the aperture size, then the breakdown characteristic had a pd dependency (p being the ambient gas pressure). The parallel-plate system has such a dependency. This implies that the aperture has no role in the discharge. However, when d is less than $3D$ then the discharge has a p^2dD dependency implying that the aperture plays a role. It has been well determined that in a typical pseudospark device that the initial electrons originate from the hollow cathode.[1,11] This mandates the use of a geometry where the aperture in the hollow cathode plays an important role. When the scaling law is applied to an individual gap of a multigap system with a thickness of 1.3 cm, an aperture size of 0.635 cm satisfies the condition that d is less than $3D$.

In the final design, a six gap system was chosen with aperture size 0.635 cm, insulator thickness (gap distance) 1.3 cm, and the thickness of the individual electrodes 0.32 cm. The diameter of the electrode was 7.62 cm and the diameter of the insulator was 9.53 cm. The reason for this small diameter was the ease of fabrication of the insulators and floating electrodes. Near the triple point, the insulator interface is not straight but has a 135° angle with respect to the floating electrode closer to the hollow cathode. This is done to increase voltage standoff.[12]

To boost the capacitance of the system, a low-inductance parallel-plate capacitor was used. One plate was directly attached to the cathode and the tank wall formed the other plate. The plate that was attached to the cathode was made out of a glass epoxy (G10) board with copper stripped from the side facing the tank. The total capacitance of the system was 80 pF. A picture of the assembly is shown in Fig. 2. Suitable high-voltage grading rings are attached to the external parallel-plate capacitor.

C. Trigger circuit and assembly

A trigger system was designed, whereby the discharge was initiated by having a small flashover between a trigger electrode and the surrounding wall of the cathode. Figure 3 shows the trigger electrode in the hollow cathode. The trigger circuit is shown in Fig. 4. The potential difference between the 100% and 75% taps present on the pulse transformer is used to trigger the circuit as shown in Fig. 3. A 500 pF, 30 kV high-voltage capacitor is charged through the charging resistor (9 kΩ), a 2 kΩ resistor, and then finally through a 50 kΩ resistor to the 75% tap. The charged capacitor, a small spark gap, and the trigger electrode/cathode

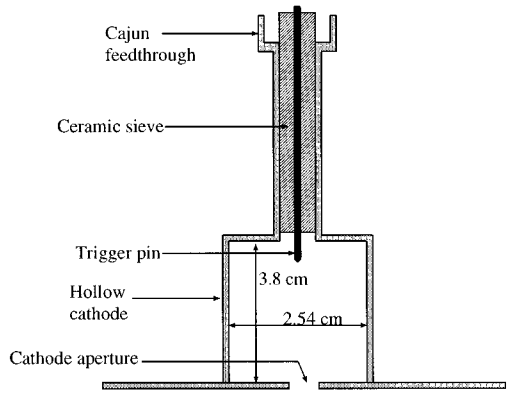

FIG. 3. Hollow cathode with the trigger pin.

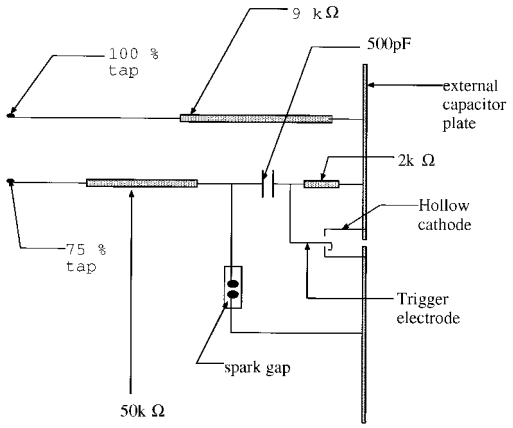

FIG. 4. The trigger circuit. The 500 pf capacitor is charged by the voltage difference between the 100% and 75% taps of the pulse transformer. The voltage on this capacitor is applied between the trigger electrode and cathode housing to effect a trigger. The small spark gap is used to control the timing of the trigger.

housing constitute the local trigger circuit. When the spark gap closes (the time when it does relative to the main pseudospark charging pulse can be controlled by changing the gas pressure in the spark gap), the entire voltage of the charged capacitor is applied to the trigger electrode/cathode housing. It can be shown that the voltage on the 500 pF capacitor is given by the following equation:

$$V_c(t') = \frac{V' t'}{\tau} - \frac{V' RC}{\tau}\,(1 - e^{-t'/RC}). \tag{1}$$

Here t' is the instance when the small spark gap closes, RC is the time constant of the trigger circuit (30.5 μs), and V' is the peak of the voltage difference between the 100% and the 75% taps. The voltage between these taps has been modeled as a ramp with a rise time of about 13 μs. Therefore, if the peak charging voltage of the pseudospark is 400 kV in 13 μs, the voltage on the 500 pF capacitor is about 20 kV. This is sufficient with the field enhancement provided by the pointed trigger electrode to flash over introducing seed electrons in the hollow cathode.

D. Diagnostics

An exit wall current monitor (fast current transformer) was used to measure the total electron current ejected out from the downstream end of the device. A Faraday cup was also used to measure the total beam current as a function of distance along the system axis. A capacitive voltage divider monitors the voltage at the output of the transformer and a $\dot{D}$ probe monitors the pseudospark voltage. A Pirani gauge was used to measure the ambient gas pressure in all experiments. In addition, special diagnostics were constructed to characterize the electron-beam energy and spot size. These are described in later sections.

III. EXPERIMENTAL RESULTS

The experimental results in this section have been divided into two categories those related to the pseudospark discharge and those related to the characterization of the electron beam. Under the first category experiments related to the establishment of the left-hand operation, type of fill gas, and role of the trigger are briefly described and in the second category experiments related to the characterization of the electron beam are described.

A. Pseudospark discharge

1. Left-hand side operation

Generally, for a parallel-plate system, the Paschen minimum occurs around $pd = 0.75$ Torr cm for most gases.[1] This pd value has been used as a rough guide to establish left-hand side operation. The multigap pseudospark operated in the regime where pd was on the order of 0.4 Torr cm. A confirmation of operation in the left-hand side was provided by the following experiment. Initially, an attempt was made to feed the gas directly to the hollow cathode side; however this resulted in the discharge taking place in the gas tube instead of the pseudospark device. This clearly established the fact that the pressure regime was along the left-hand branch of the breakdown curve (long-path breakdown). Figure 5 shows the voltage at which the discharge begins versus p^2d for a six gap and eight gap system in neon. The voltage has been plotted against p^2d rather than pd as the pseudospark onset voltage has a p^2d dependence[10] for a fixed aperture diameter D. Even though the use of a trigger alters the actual breakdown characteristic, the curve shows left-hand operation (rising voltage with decreasing p^2d). Figure 6 shows a typical voltage trace at the transformer output (monitored by a capacitive divider, peak voltage 400 kV). The trigger manifests as a spike on the voltage waveform. Notice the slow voltage rise and the sudden voltage collapse.

2. Fill gas

In the pulse line experiments[7,9] argon was used as a fill gas; however, for higher voltages ($>$200 kV) argon was not satisfactory as the ambient pressure was low (18–27 mTorr) and the operation erratic. Neon and helium were both tried because, for a given voltage and a given anode cathode distance, the ambient pressure of neon (35–50 mTorr) is greater

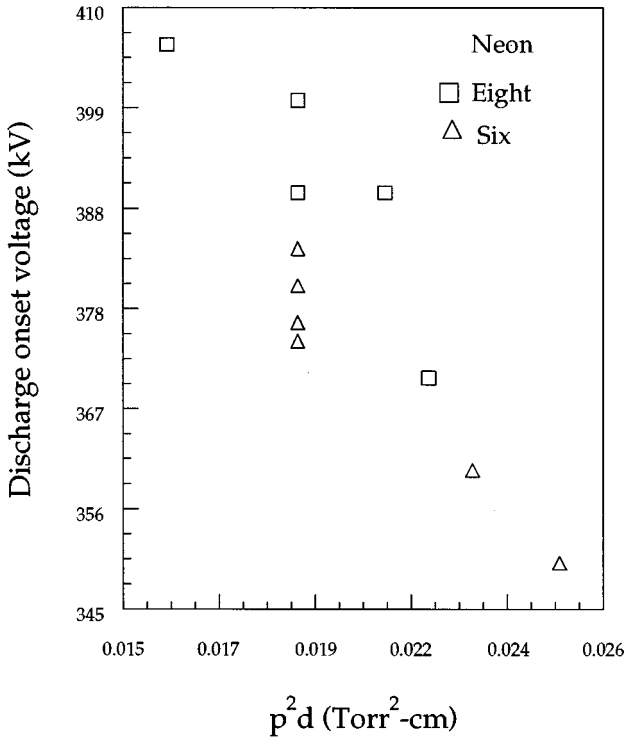

FIG. 5. Voltage (when the discharge begins) vs p^2d for a six and eight gap system in neon.

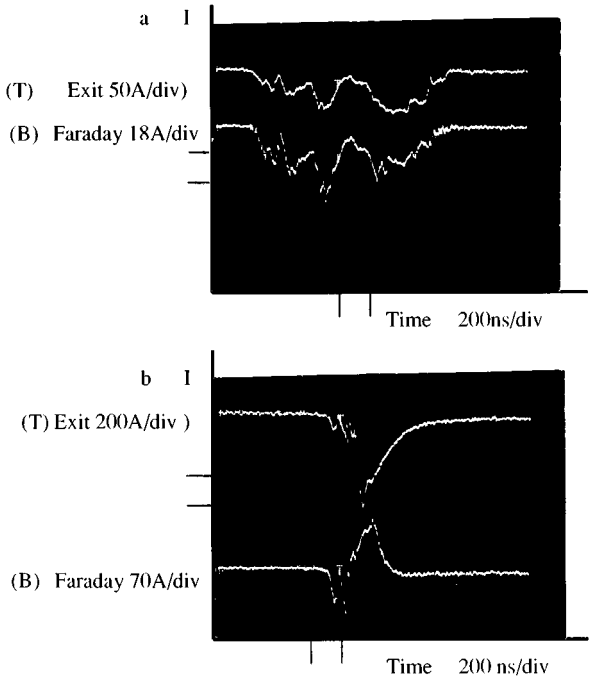

FIG. 7. (a) Electron-beam current trace for He at 360 kV. Top: Exit current monitor I_{max} 90 A (50 A/div); bottom: Faraday cup peak 56 A (18 A/div). (b) Electron current trace for Ne at 360 kV. Top: Exit current monitor I_{first} 120 A, I_{max} 600 A (200 A/div); bottom: Faraday cup I_{first} 85 A, second peak 140 A (70 A/div). The faraday cup was placed about 15 cm from the anode aperture.

than that of argon, and that of helium (98–110 mTorr) is greater than that of neon. However, neon was finally chosen, because the electron beam current for neon was much higher than that for helium. Figure 7(a) shows the electron-beam trace for helium at 360 kV (top: wall current monitor at the anode exit; bottom: the Faraday cup 15 cm away from the anode) and Fig. 7(b) shows the electron-beam trace for neon (top: wall current monitor; bottom: Faraday cup). Notice that in the case of helium, the electrons are ejected out in several phases. Currents associated with the first peak are on the order of 40–50 A and the second peak on the order of 90 A. In the case of neon there are three distinctive features on the current wave form: There is the initial current peak between 120 and 160 A, then the second peak between 200 and 220 A and finally there is the biggest peak (400–800 A). It is shown in the following subsection (energy measurement) that the initial peak is associated with the full voltage, the second peak has lesser energy (150–200 keV), and the third peak (max peak) is basically very low-energy electrons (plasma electrons). Moreover, evidence on copper foil targets shows that in the case of helium the electrons are not strongly pinched unlike the case of neon. The main reason for this difference in behavior between helium and neon can be attributed to the difference in atomic mass number and different ionization potentials (helium has higher ionization potential and is lighter than neon). For pinching to take place charge neutralization is required without current neutralization. It is possible that the lighter helium ions move resulting in a partial cancellation of the current.

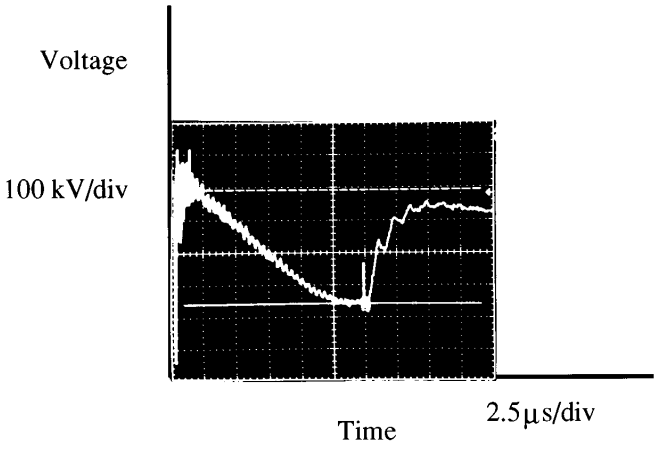

FIG. 6. Typical voltage trace at the transformer output (100 kV/div) with the trigger shown as a spike before collapse. Time scale 1 div: 2.5 μs.

3. Role of the trigger

There are two main reasons behind the decision to trigger the high-voltage pseudospark device. First, the trigger is very important in a device like ours which is pulse charged and where the general ambient pressure is rather low. The device is subjected to jitter due to the finite duration of the pulse. Second, the triggering of this device ensures that the discharge originates in the hollow cathode.

TABLE I. Ejected electron-beam current magnitude in the first and second peak for different charging voltages and delays (time interval between trigger and collapse of voltage). Here τ represents the duration of the current (first peak and second).

V (kV)	Delay (μs)	I_{1st} (A)	τ (ns)	I_{2nd} (A)	τ (ns)
350	<1	120	120	200	100
350	<1	80	100	200	120
350	2.5	160	100	200	130
360	<1	120	80	200	120
374	2	160	120	200	160
384	<1	120	80	200	120

Typically, the voltage collapse begins 1–2 μs after the trigger. Also, the duration of the first peak is a function of the time interval between the trigger and the onset of the voltage collapse. Typically, the duration is greater (duration of the first peak is of the order of 100 ns) for larger time intervals between the trigger and onset of the discharge. In general, the triggering of the device results in an increase of the current of the first peak and also the duration of the first peak. These results are summarized in Table I.

B. Electron-beam characterization

1. Energy analysis

In order to determine the beam energy, electron range-energy studies were undertaken. For these studies, a range-energy probe was made with self-integrating Rogowski coils on both sides to measure the incident and transmitted current simultaneously. Figure 8 shows the incident and transmitted electron-beam current when it hits a 1 mil (0.0025 cm) aluminum foil. Notice the pulse shortening of the incident beam. The photograph clearly indicates that the high-energy electron beam occurs early in time like the pulse line pseudospark experiment.[9] Aluminum, copper, and tantalum foils were used as stopping foils. In Fig. 9 the percentage transmitted current versus thickness is plotted for the first peak in aluminum at 360 keV. Notice that the experimental points

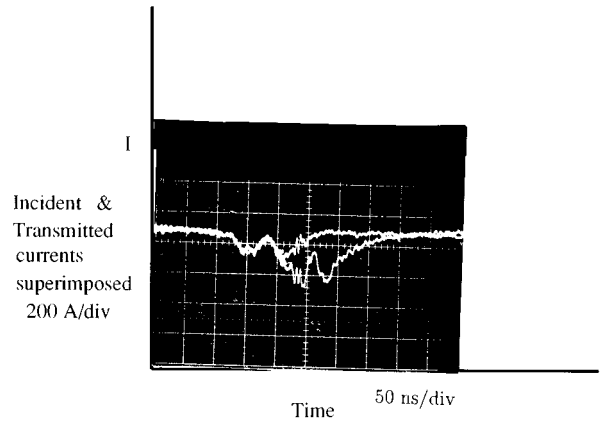

FIG. 8. Incident (I_{first} 160 A) and Transmitted (I_{first} 130 A) electron-beam current through a 0.0025 cm aluminum foil. The wave forms are superimposed. The vertical scale is 200 A/div and the horizontal time scale is 50 ns/div.

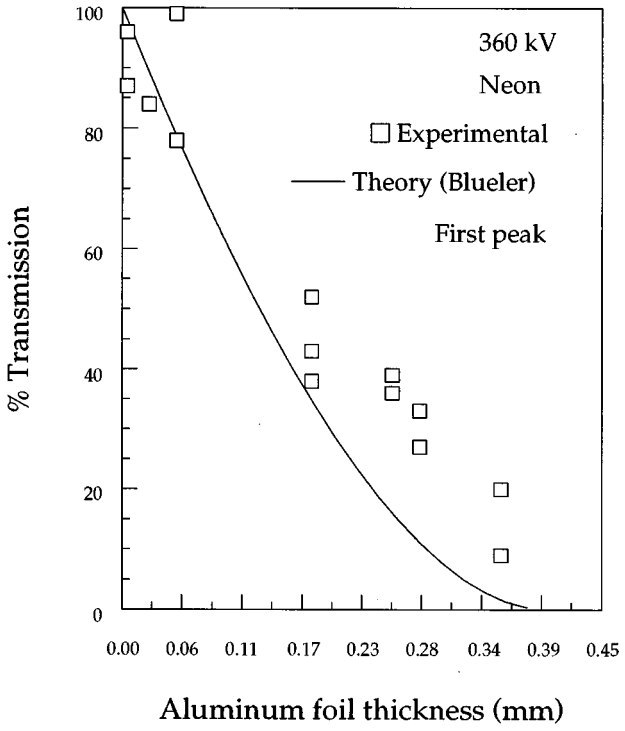

FIG. 9. Percentage transmission (theoretical and experimental) vs thickness (aluminum) for the initial electrons (first peak). The theoretical curve was derived using monoenergetic electrons of energy 360 keV. The close match between theoretical and experimental values suggests that the initial electrons have energy comparable to the full charging voltage (360 kV).

are compared with the theoretical curve based on the formula derived by Bleuler and Zunti.[13] The transmission defined as the fraction N/N_0 of the initial intensity remaining in a homogeneous beam of electrons (initial energy E_0) after traversing a distance x_0 through an absorber is

$$\frac{N}{N_0}=\exp\left(-\int_0^{x_0}\alpha(x)dx\right), \tag{2}$$

where

$$\alpha(x)=14.2\left(\frac{E(x)+0.511}{E(x)[E(x)+1.022]}\right)^2 \ \text{cm}^{-1}. \tag{3}$$

Here $E(x)$ is the energy in MeV of the electrons after passing through a thickness x and is related to x in the following manner:[14]

$$E(x)=1.92[R(x)^2+0.22R(x)]^{0.5}, \tag{4}$$

where

$$R(x)=R_0-2.7x, \tag{5}$$

$$R_0=0.5\left(0.0484+\frac{4E_0^2}{3.684}\right)^{0.5}-0.11. \tag{6}$$

The distance $2.7x$ is expressed in g/cm^2 (range units) for aluminum (density 2.7 g/cm^3). R_0 is the theoretical range for monoenergetic electrons of energy E_0 in aluminum. The theoretical curve compares very well with the experimental points confirming the fact that the initial peak is at the energy

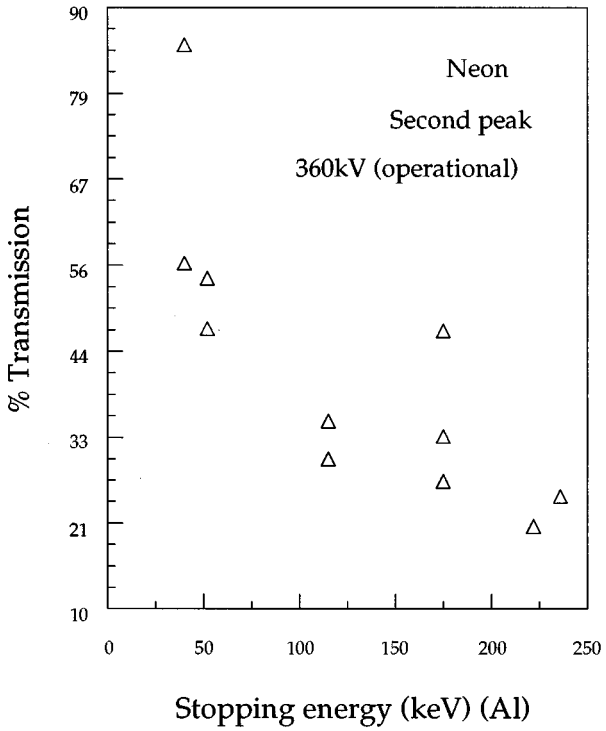

FIG. 10. Percentage transmission of electron-beam current vs stopping energies (corresponding to different foil thickness of aluminum) for the second peak. The charging voltage is 360 kV.

equivalent of the full charging potential of the pseudospark (360 kV in this case). Figure 10 shows the percentage transmission at different stopping energies of aluminum foils (varying thickness) for the second peak. Here the stopping energy corresponds to the energy of the equivalent monoenergetic electron beam for which the given thickness of aluminum constitutes the range. Therefore, a significant transmission at a given energy would imply the presence of electrons with energy higher than the stopping energy. It is clear from this figure that the electrons in the second peak are quiet energetic though at a lesser energy compared to the first peak. Energy analysis with the other foils was consistent with the range-energy results for aluminum. In Fig. 11 the scanned electron microscope image of the damage on a 0.2 mm copper sheet is shown. There is a large spot (diameter 1 mm) and a small spot (diameter 0.200 mm) to the right-hand side. It is believed that the large spot damage due to higher-energy electrons and the small pinched spot seen to the right-hand side of the large spot is due to lower-energy electrons which originate later in time. The experiments describing spot size imaging using an x-ray pinhole camera (described in the following subsection) also appear to confirm the assertion.

2. Spot-size imaging

In this experiment, an x-ray pinhole camera (see Fig. 12) is used to determine, the spot size of the beam. The aim in this experiment is to establish that the strongest pinching occurs later in time and is associated with the lower-energy electrons. Basically the electron beam impinged on a

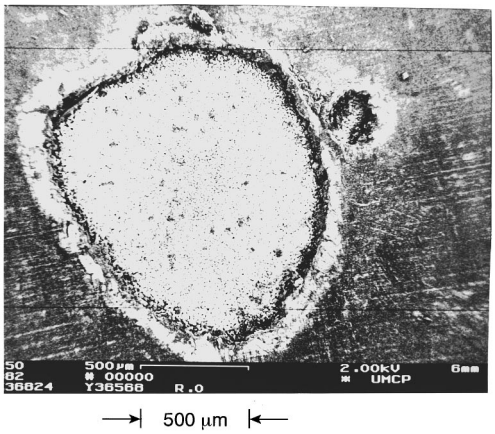

FIG. 11. Scanning electron microscopy image of the damage on a 0.2 mm copper foil. Notice the large spot and a smaller spot to the right-hand side. The scale length is indicated on the photograph.

''thick'' target of tantalum (high-Z material). A target is defined as thick if the scattering and energy loss processes would have an appreciable effect on the energy of the electron beam. X rays were produced locally on an area comparable to the spot size of the electron beam. The source was then imaged onto an x-ray phosphor screen (gadolinium oxysulphide deposited on a glass) through an array of nine pinholes forming multiple images.

Initially, a magnification of 1 was used between the source plane (target) and the image plane. A tantalum foil of 2 mil (0.0051 cm) was used as the target (~8 cm from the anode and charging voltage of 360 kV). Figure 13(a) shows an initial image with a small camera aperture. Nine images are seen. Based on this image size, the spot size is about 0.5 mm (diameter). This image suggests the pinching of the beam. In Fig. 13(b), the photograph is taken with a larger aperture. In each image (corresponding to each pinhole) a large bright spot (on the order of 1.5–3 mm) and a smaller but more intense spot (0.5 mm) is seen. This image clearly establishes that the pinching occurs separately. In order to determine if the brighter spot is of higher energy, a piece of copper foil (0.075 mm) effectively blocking some of the pinhole images was placed very close to the phosphor screen.

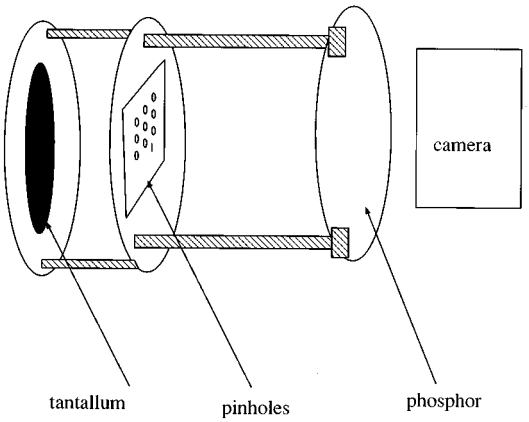

FIG. 12. X-ray pinhole camera.

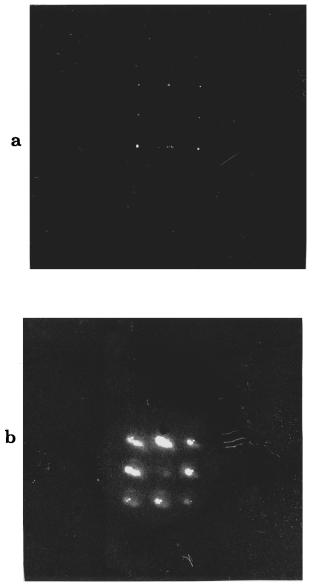

FIG. 13. (a) Source images with very small camera aperture spot size 0.5 mm; (b) source images with larger camera aperture. In each image a large bright spot (1.5–3 mm) and a smaller but more intense spot (0.5 mm) is seen.

This copper foil has a 50% transmission for photons of energy equal to 30 keV. Figure 14(a) shows a photograph with small apertures. Notice that only the images of the pinholes not covered by the copper foil are seen. The beam appears to be pinched. In Fig. 14(b), the aperture of the camera is larger. The source images through the copper foil are seen. The images appear larger than the pinched small diameter

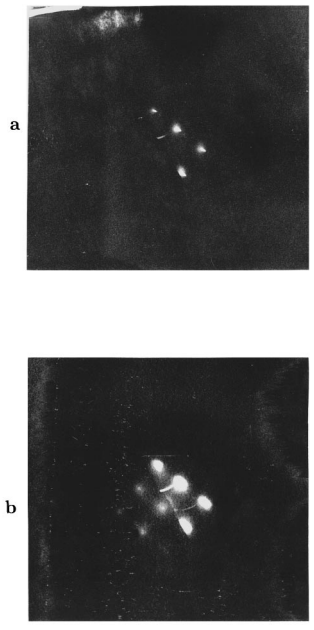

FIG. 14. (a) Source images with pinholes partially covered with copper foil (0.075 mm) and small camera aperture; (b) source images with pinholes partially covered with copper foil (0.075 mm) and large camera aperture. The images are seen through the copper foil. The images through the copper foil do not appear pinched indicating that the higher-energy electrons are not pinched.

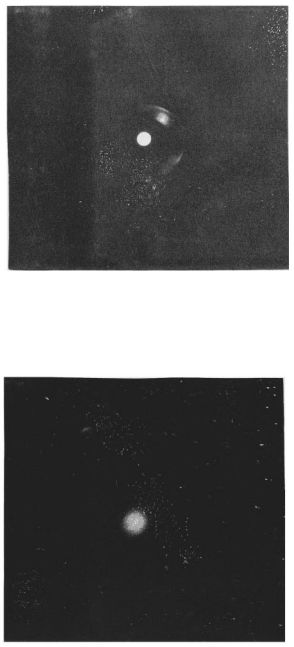

FIG. 15. Mylar witness plate: (a) Image of the electron beam after it transmits through a 0.051 mm Tantalum foil, (b) image of the electron beam after it passes through a 0.10 mm Tantalum foil.

images seen in Fig. 14(a). These photographs indicate that the strongest pinching occurs later (because the energy of the x-ray photons appear to be lower). Note, however, that the photographic images are time integrated.

3. Mylar as a witness plate

In this experiment a novel imaging technique of using a thin Mylar foil of thickness 1 mil (0.0254 mm thick) to monitor the electrons after being scattered by a 2 mil (0.051 mm) tantalum foil (stopping energy 200 keV) and a 4 mil (0.10 mm) (stopping energy 325 keV) was employed. Intense light proportional to the beam current and diameter (due to luminescence[15]) was emitted. The mechanism of light emission is not cherenkov emission because the electrons after passing through range-thick target foils are not relativistic. Figure 15(a) shows an image of the electron beam after it hits a 0.051 mm tantalum foil. The true size of the image is on the order of 0.48 cm. While the large diameter of the image can be attributed to the scattering processes, the sharpness of the image seem to indicate that the beamfront is axisymmetric. This is again reinforced in Fig. 15(b) which shows the image of the beam after transmission through a 0.102-mm-thick tantalum foil (spot size 0.863 cm). Caution should, however, be exerted in that the response of the film (Polaroid 667) to this light is not known.

4. Shot reproducibility

A series of shots was taken repeatedly on a 0.2 mm copper sheet (stopping energy 400 keV) placed 8 cm away from the anode hole to see if the beam wandered in position, shot to shot. The damage pattern on the 0.2 mm copper sheet revealed that there was very little variation in position. The

damage due to these shots lay in a circle of diameter 0.254 cm. Generally, single shot damage on range-thick targets resulted in two spots. There was, as previously mentioned, a larger diameter ($\sim$1 mm) spot and a smaller spot (diameter $\sim$0.2 mm) which varied in its position. Sometimes this spot lay on top of the larger spot and sometimes adjacent to it. This was also seen in the x-ray pinhole images (see Fig. 13, bottom).

IV. DISCUSSION OF RESULTS

Considering the various experimental evidence of damage on copper foil, x-ray pinhole images, and Mylar imaging, it is almost a certainty that the initial electrons are not pinched and strong pinching occurs only later in time when a plasma channel is established. The picture that emerges is the following. The initial electron beams feeling no pinch effect are of larger diameter. The beam electrons are held together primarily by the the relativistic nature of the beam. Later in the beam pulse, as the plasma channel develops, the pinch is fully developed. There are several important issues associated with pseudospark operation that merit attention. First, the process of electron-beam generation and propagation through gas are intimately linked from the hollow cathode to the anode exit hole and beyond. The fact that the initial electrons are at energy equivalent to the full anode cathode voltage (350–400 keV) when measured 8 cm away from the anode, seems to indicate they suffer very few collisions (mean-free-path lengths are on the order of meters[3]). The initial burst constitutes these runaway electrons. This implies that the lower-energy electrons which evolve later in time are involved in the establishment of the plasma channel as the electron–neutral ionization cross sections are very large for lower energies. An estimate of the number density of the electrons in the initial peak using the following typical numbers for current (160 A), energy 360 keV, and diameter of the beam ($\sim$3 mm) is 5.8×10^{11} cm^{-2}.

In this series of experiments, an accurate estimate (experimental) of the spot size ($\sim$3 mm) of the high-energy electrons along with the associated current is known ($\sim$160 A). In our earlier experiment,[9] we had reported energy-invariant normalized emittance values for the initial high-energy electrons. These values lie in the range 30–80 mm mrad. Therefore, an estimate of the brightness should lie in the range $0.5–3.6\times10^{10}$ A/m^2 rad^2.

The pseudospark-generated electron beam has a large longitudinal energy spread (over time). To use such an electron beam as an electron source for high-power microwaves is difficult. It would be necessary to establish a method to filter out electrons which originate later in time (lower energy) without disturbing the beam transport. This would be difficult considering the fact that some of the electrons originating later in time still have considerable energy. This experiment, however, presents an unique opportunity to study beam plasma interaction as the energy of the electrons fall in time. This may be of interest in the development of a physical model to describe processes which accompany the polar aurora formation. Considering the axisymmetric damage on metal targets, the electron beam could be used for materials processesing. The overall diameter being still small, the distinction between the spot sizes of the electron beams originating at different times may not be important.

V. CONCLUSIONS AND FUTURE WORK

This article reports on the design and execution of a high-voltage triggered pseudospark experiment. The major conclusions that can be drawn from this work are as follows.

The role of geometry and aspect ratio in the scaling of low-voltage pseudospark experiments to a high-voltage experiment have been confirmed. A multigap pseudospark device was designed and built which operated reliably in the voltage range 300–400 kV.

For this device neon as a fill gas was found to be better suited than helium as far as electron-beam generation was concerned.

The electron beam was generated in several stages. The initial burst of electrons (120–160 A) was found to have energy equivalent to the full anode–cathode potential. The electrons which were generated later in time also had substantial energy although less than the initial peak.

Strong pinching was associated with the electrons which were generated later in time. The initial high-energy electron beam is larger in diameter. This was confirmed using source-size imaging techniques employing both an x-ray pinhole camera and the luminescence with passage of electrons through thin Mylar foils.

Future experiments are planned in which the pseudospark generated electron beams will be used to generate microwaves. Also, the inherent capacitance of the device will be boosted by increasing the diameter of the electrodes and insulators.

ACKNOWLEDGMENTS

We would like to acknowledge useful discussions with Professor M. J. Rhee, Chengjun Liu, and Girish Saraph. It is also a pleasure to acknowledge the technical support of Jay Pyle and Doug Cohen. This work was supported by the U.S. Department of Energy.

[1] J. Christiansen and Ch. Schulthheiss, Z. Phys. A **2990**, 35 (1979).
[2] M. Höbel, J. Geerk, G. Linker, and C. Schultheiss, Appl. Phys. Lett. **56**, 973 (1990).
[3] R. Stark, J. Christiansen, K. Frank, F. Mucke, and M. Stetter, IEEE Trans. Plasma Sci. **PS-23**, 258 (1995).
[4] K. K. Jain, E. Boggasch, M. Reiser, and M. J. Rhee, Phys. Fluids B **2**, 2487 (1990).
[5] W. Benker, J. Christiansen, K. Frank, H. Gundel, W. Hartman, T. Redel, and M. Stelter, IEEE Trans. Plasma Sci. **PS-17**, 754 (1989).
[6] P. Choi, H. H. Chuaqui, M. Favre, and E. S. Wyndham, IEEE Trans. Plasma Sci. **PS-15**, 248 (1987).
[7] W. W. Destler, Z. Segalov, J. Rodgers, K. Ramaswamy, and M. Reiser, Appl. Phys. Lett. **62**, 1739 (1993).
[8] J. Zhu, Z. Wang, L. Zhang, and M. Wang, IEEE Trans. Plasma Sci. **PS-24**, 161 (1996).
[9] K. Ramaswamy, W. W. Destler, Z. Segalov, and J. Rodgers, J. Appl. Phys. **75**, 4432 (1994).
[10] C. J. Liu and M. J. Rhee, IEEE Trans. Plasma Sci. **PS-23**, 235 (1995).

[11] J. P. Boeuf and L. C. Pitchford, IEEE Trans. Plasma Sci. **PS-19**, 286 (1991).
[12] N. C. Jaitly and T. S. Sudharshan, IEEE Trans. Electr. Insul. **EI-22**, 801 (1987).
[13] E. Bleuler and W. Zunti, Helv. Phys. Acta **19**, 375 (1946).
[14] L. Katz and A. S. Penfold, Rev. Mod. Phys. **24-1**, 28 (1952).
[15] V. I. Krementsov, P. S. Strelkov, and A. G. Shkvarunets, Sov. Phys. Tech. Phys. **25**, 1447 (1980).